1   **The catastrophic landfill flowslide at Hongao dumpsite on December 20, 2015 in Shenzhen, China**

2   Qiang Xu[1], Dalei Peng[1], Weile Li[1], Xiujun Dong[1], Wei Hu[1], Minggao Tang[1], Fangzhou Liu[2*]

3   [1]State Key Laboratory of Geohazard Prevention and Geoenvironment Protection, Chengdu University of
4   Technology, Chengdu 610059, China
5   [2]School of Civil and Environmental Engineering, Georgia Institute of Technology, Atlanta, GA, USA

6   **Abstract** A catastrophic flowslide occurred at Hongao dumpsite at approximately 11:40 AM on Dec 20,
7   2015, in Guangming New District of Shenzhen, China. The flowslide damaged 33 buildings and caused
8   total death toll of 69 and 8 missing, with the absence of extreme weather condition and seismic activity.
9   The slope failure was analyzed on the basis of multi-temporal remote sensing images, site investigation, *in-
10   situ* tests, laboratory experiment, and numerical analysis. The preliminary results showed that the volume
11   of the flowslide deposit was 2.32×10^6 m^3 and the volume of dumpsite filling was 6.27×10^6 m^3 at the time
12   of the event, which is three times larger than the maximum design capacity. The flowslide had the
13   characteristics of high travel speed and long run-out distance, of which the displaced material was primarily
14   silty soil from nearby construction sites with high moisture content. The primary causes of the failure were
15   concluded as follow: (1) The dumpsite stagnated groundwater flow in the study area, which resulted in the
16   saturation of the waste filling and high pore water pressure due to the underlying impermeable granite
17   stratum; (2) The accumulation rate and total volume of the waste filling was in exceedance of the design
18   capacity. The slope failure may be ascribed to excess pore water pressure as liquefaction were observed at
19   many locations and it is postulated that such phenomena was related to the surcharge loads imposed by the
20   unregulated disposal activities.

21   **Keywords** Flowslide, Landslide, Municipal Solid Waste (MSW), Dumpsite, Quarry, Landfill

22   **1 Introduction**

23   Owing to the rapid population growth and industrialization, increase in the accumulation rate of municipal
24   solid waste (MSW) poses challenges in MSW management and urban planning (Huang and Cheng 2016).
25   Landfilling is the most common method of MSW disposal management (Brunner and Fellner 2007; Huang
26   and Cheng 2016). Transformation of an abandoned quarry to a MSW dumpsite is a general approach as it
27   conserves resources by reclaiming the quarry space and provides MSW storage solution (Zou 2016). The
28   landfill slope stability is critical in MSW management, and therefore, the selection and design of landfills
29   require engineering assessment on slope stability and environment impact (Zou 2016).

30   The porosity and moisture content of MSW is typically high in unregulated landfills due to inadequate
31   drainage system. Therefore, the residual soils in MSW may exhibit fluid flow behave, i.e. flow slide, with
32   extremely high mobility in the event of a slope failure (Dai et al 2016; Huang and Cheng 2016). Study on
33   the landfill slope failure in MSW dumpsite can be found in previous literatures, of which 6 reported cases
34   between 1993 and 2005 resulted in around 500 deaths and significant properties loss (Mitchell et al 1990;
35   Kjeldsen and Fischer 1995; Kocasoy and Curi 1995; Eid et al 2000; Blight and Fourie 2005; Merry et al
36   2005; Yılmaz and Atmaca 2006; Blight 2008). The deadliest event in history killed 278 people in Manila,
37   Philippines in 2000, and the second deadliest event buried 71 houses and killed 143 people on Feb 21, 2005
38   at Leuwigajah dumpsite near Bandung, Indonesia, (Lavigne et al 2014).

39   Shear strength of MSW is a function of various parameters, such as waste type and composition, disposal
40   rate, moisture contents, overburden pressure, and compaction (Eid et al 2000; Huvaj-Sarihan and Stark
41   2008). The movement of waste avalanches are complex and still poorly known (Lavigne et al 2014) due to
42   the lack of field monitoring data. The existing studies have focused on empirical methods (e.g. Blight and
43   Fourie 2005; Srour 2011), laboratory experiment, and numerical analysis. An approach was presented to
44   estimate the maximum flow velocity of MSW slope failure based on energy balance (Blight and Fourie
45   2005). The empirical-statistical method still has widespread use in practical applications, but the accuracy
46   is often model dependent (Dai et al 2016; Huang and Cheng 2016). The mixture of peat, kaolinite, and
47   quartz sand were used in laboratory tests to simulate MSW landslide, of which the results shown that, with

48 increased moisture content of the MSW, the mobility increases while the maximum and final flow depth
49 decrease (Dai et al 2016). Numerical simulation has been widely used in the landfill slope stability analysis
50 (Chang 2002; Chang 2005; Chugh et al 2007; Chen and Yuan 2009; Huang et al 2013; Huang and Cheng
51 2016). The Smoothed Particle Hydrodynamics (SPH) method was used for run-out distance analysis of two
52 typical landfill flow slides occurred in Sarajevo and Bandung (Huang and Cheng 2016).

53 A MSW slope failure occurred at Hongao dumpsite, Guangming New District of Shenzhen, China at 11:40
54 AM on Dec 20, 2015, which destroyed 33 buildings and accommodations in the adjacent industrial park,
55 and resulted in death of 69 with 8 missing as of Jan 12, 2016. No extreme weather conditions or seismic
56 activity were reported at the time of the event. This article aims at investigating the characteristics and
57 causes of the flowslide. Field investigation, *in-situ* test, UAV stereo-measurements, and remote sensing
58 image interpretation were applied to recover material properties and landform characteristics of the study
59 area. Laboratory experiment and numerical analysis were performed to improve understanding on the
60 failure process.

61 **2 Data and Methodology**

62 **2.1 Satellite Images, Topographic Map, and Aerial Photo**

63 A series of high resolution satellite images was identified on Google Earth between Nov 2002 and Feb
64 2016. A Pleiades remote sensing image of the study area obtained on Dec 18, 2015 (2 days before the event)
65 was used to facilitate the analysis (Fig. 1a). Topography map of the pre-disposal site was provided by the
66 local government, and the drawing was submitted by a third-party consulting firm in Dec 2013. According
67 to the project report, the designed waste filling storage of was 2×10^6 m^3 with 10 slope benches at a ratio of
68 1:2.5. Aerial photos with resolution of 5 cm were collected by an Unmanned Aerial Vehicle (UAV) 3 days
69 after the flowslide (Fig. 1b). The Digital Orthoimage Map (DOM) and Digital Surface Model (DSM) were
70 reconstructed from the aerial photos, and a topographic map for the post-sliding dumpsite was generated
71 from the DSM at the scale of 1:1000. As shown in the Pleiades image taken (Fig. 1a), a structured terrain
72 for vehicles was excavated for around the pre-sliding dumpsite consisting of 8 benches and 3 platforms.
73 The topographic map for the pre-sliding dumpsite was derived by overlaying the image of the original, pre-
74 sliding, and post-sliding slopes, which provided estimation on the volume and depth of the pre-/post-sliding
75 landfill.

76 **2.2 Field Investigation and *in-situ* Tests**

77 The first field investigation was conducted on Dec 23, 2015 and second investigation was deployed between
78 Jan 21 and Jan 25, 2016. Field investigations assessed the topographical, geological, and groundwater
79 conditions. The density, moisture content, and permeability of the displaced material of the flowside was
80 measured from *in-situ* tests. The material properties were used in the subsequent laboratory experiment and
81 numerical analysis.

82 **2.3 Laboratory Tests**

83 Undisturbed and disturbed soil samples were obtained for laboratory tests, including weathered silty soil
84 and waste filling from the dumpsite. Grain size analysis was conducted by using the wet sieve method with
85 sieve sizes of 20, 10, 5, 2.0, 1, 0.5, 0.25, 0.10, 0.075, 0.025, 0.01, 0.005, 0.002, and 0.001 mm. The
86 maximum dry density and optimum moisture content of the displaced material were determined from the
87 standard laboratory compaction test. The shear strength parameters of the displaced material (c, Φ) were
88 obtained by triaxial compression test.

89 **2.4 Numerical Analysis**

90 In order to analyze the stability of the dumpsite, input parameters for the material properties and model
91 geometry were same as the corresponding values measured on site or in the laboratory. Factor of Safety
92 (FOS) of the slope was calculated by using SLOPE/W software with Morgenstern Prince Limit Equilibrium
93 Analysis method.
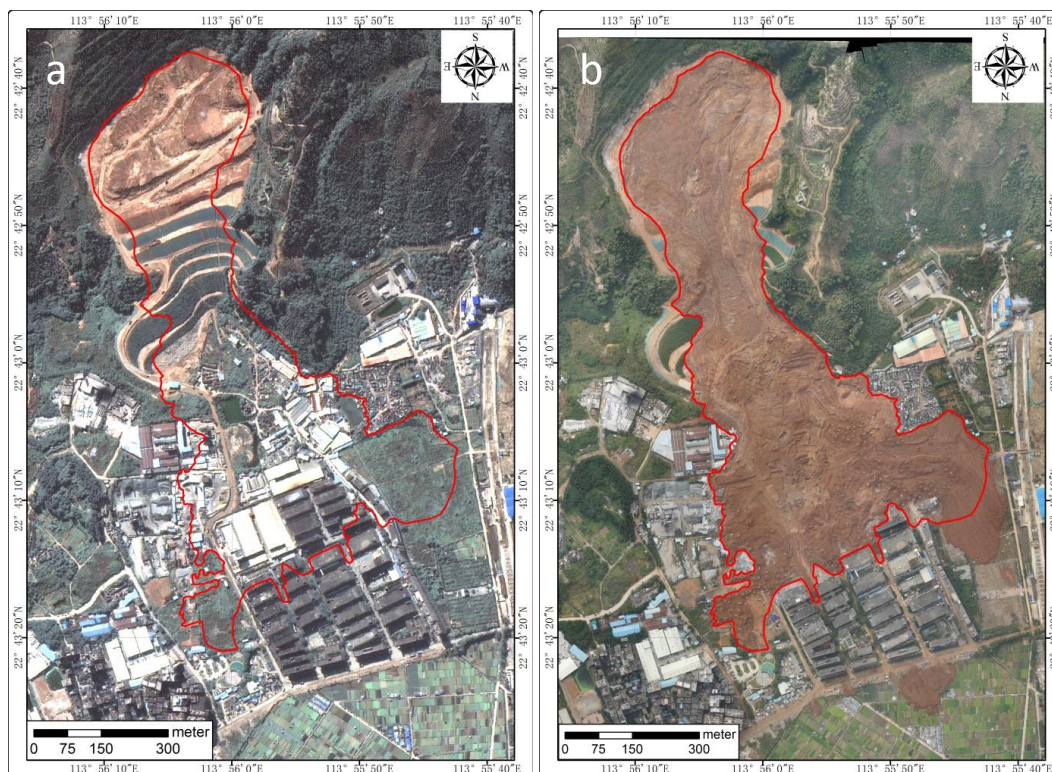
94

95 Fig. 1 Images for the Pre- and Post-sliding dumpsite. The boundary of the flowslide is indicated by the red
96 line. **a** Pleiades satellite image (Dec 18, 2015); **b** Aerial photo (Dec 23, 2015).

97 **3 Geological and Climatic Setting**

98   The dumpsite is located at 23 km away from Shenzhen and 5 km away from the Guangming New District
99   (E113°56'5", N22°42'44") as shown in Fig. 2. The dumpsite was surrounded by three ridges with a free face
100 excavated with a mild slope gradient. The bedrock of the dumpsite is mainly Cretaceous granite rock (Fig.
101 3a, 3b, 3c, and 3d). The landfill consisted of construction waste with silty soil, clay, rock, and gravel (Fig.
102 3e and 3f).

103 The study area belongs to the zone of subtropical monsoon climate with an average temperature of 22° and
104 an average annual precipitation of 1500 mm concentrating between April and September (greater than 85 %
105 of the annual precipitation) (Zhang et al 2006). Based on the precipitation records from the nearby Tangjia
106 Rainfall Station between Jan 1, 2013 and Dec 20, 2015 (Fig. 5), the accumulated precipitation in the study
107 area was nearly 3240 mm, and field evidence suggested that the drainage facilities of the dumpsite were
108 abandoned (Fig. 6b and 6c), which permits the ingress of rainwater in the quarry pit (Fig. 7c). The catchment
109 area of the study area was $4.7 \times 10^5 \, \text{m}^2$, which was 2.95 times greater than the area of the dumpsite (1.6×10^5
110 m^2) as shown in Fig. 6a. Drainage system was implemented in the study area, where the surface run-off was
111 designed to be collected by the drainage pipes installed at a higher elevation than the dumpsite and divert
112 into the peripheral drainage channel. However, the drainage system failed to operate due to the absence of
113 maintenance, and led to the concentration of surface run-off and groundwater into the dumpsite. Field test
114 estimated that the permeability of the waste filling was 5.26×10^{-6} cm/s. Low permeability resulted in high
115 moisture content and excess pore water pressure in the dumpsite. The groundwater in the study area were
116 mainly bedrock fissure water and Quaternary pore water (Fig. 7).
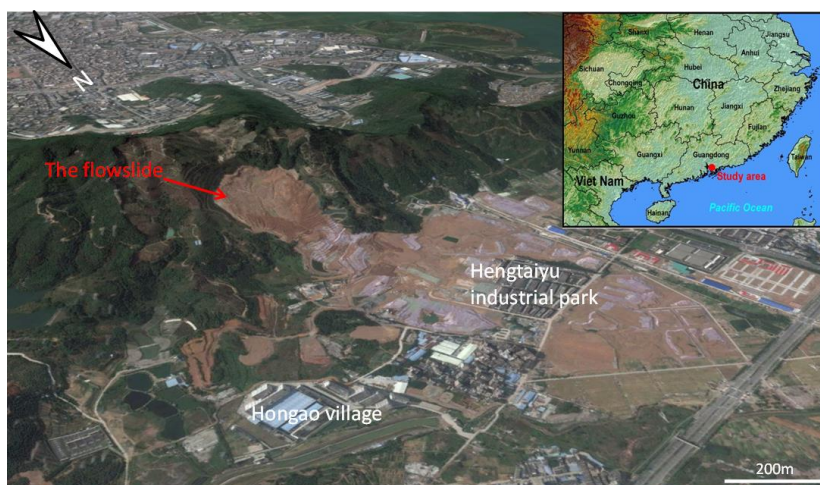
117

118   Fig. 2 Location of the study area and overview of the post-sliding dumpsite (Google Earth image taken on
119   Feb 2016).
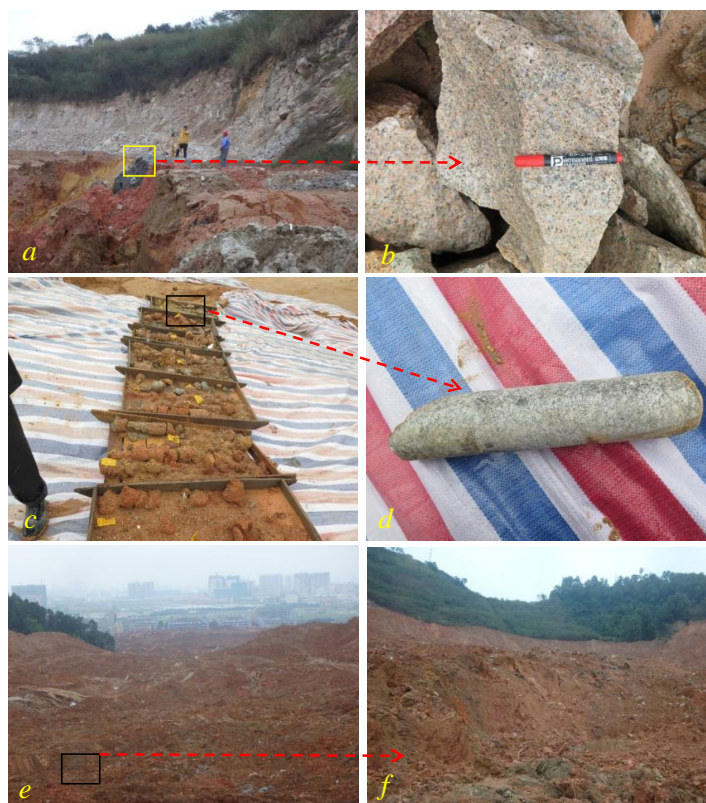
120

121   Fig. 3 Photos of the rock and soil specimen collected from the displaced material. **a** Exposed granite rock
122   near the scarp of the landslide; **b** Close view of the granite rocks; **c** Drilling core samples; **d** Close view of
123   the granite rock sample; **e** Displaced material in the zone of depletion; **f** Soils in the flowslide source area.

124
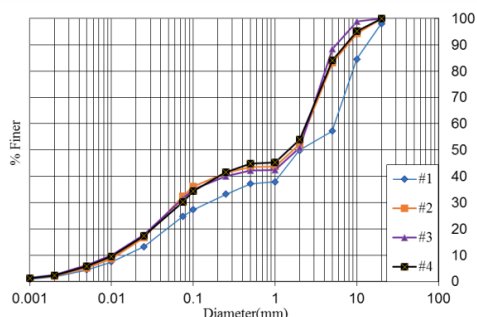
125   Fig. 4 Particle size distribution curves of the waste filling.

126
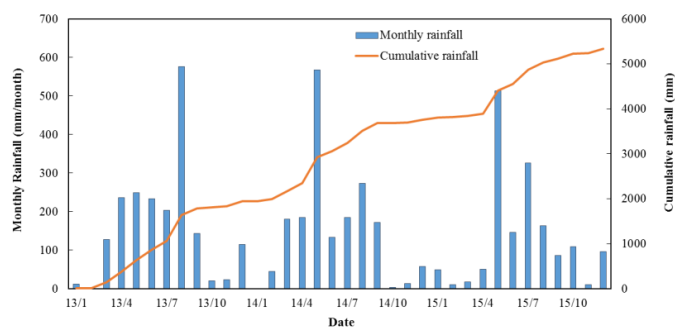
127   Fig.5 Monthly rainfall and cumulative precipitation between 2013 and Dec 2015.

128

129   Fig. 6 **a** An overview of the catchment area (Google Earth image); **b** The surrounding peripheral drainage
130   channel of the dumpsite was abandoned; **c** Damaged drainage pipes were not repaired and failed to divert
131   surface run-off into the peripheral drainage channel. Surface run-off concentrated in the waste filling.

132

133   Fig. 7 **a** Groundwater overflow in the rock fissures near the flowslide crown; **b** Water accumulation in the
134   flowslide crown; **c** Surface run-off near the flowslide source area during rainfall event; **d** Eroded channel
135   in dry condition; **e** Water accumulation in the source area; **f** Surface run-off and infiltration contributed to
136   groundwater seepage.

137   **4 Multi-Temporal Remote Sensing Images**

138   The development and changes of the dumpsite is presented by multi-temporal remote sensing images taken
139   between 2002 and 2016 (Fig. 8). It is postulated that the quarry was active between 2002 and 2008. However,
140   formation of ponds of various sizes at different spatial and temporal locations in the quarry indicated low
141   permeability and lack of drainage network (Fig. 8b, 8c, and 8d). The quarry was abandoned in or before
142   2008 as shown in Fig. 8c (obtained on 2/20/2008) with a small amount of waste filling in the quarry pit. A
143   large-scale pond was formed due to groundwater and rainfall accumulation (Fig. 8d). The depth of the pit
144   was over 100 m before the disposal activities. A service road was excavated between two rock hills exiting
145   the quarry and formed a small-scale gully cross the pit longitudinally (Fig. 8a, 8b, 8c, and 8d). Additionally,
146   a small-scale platform (abandoned office area of the quarry) was excavated at the immediate downstream
147   of quarry exit. The gully was covered during construction of a multi-bench retaining slope between the rock
148   hills as waste disposal continued throughout the process (Fig. 8e). Disposal activity was started around
149   2014 (Fig. 8e and 8f), and the accumulation rate of the waste filling was considerably fast (Zou 2016).

150 An unpaved road was excavated on the east of the quarry connecting the crest and toe of the hillslope as
151 shown in Fig. 8e. A large number of trucks can be seen transporting waste filling to the dumpsite. A large
152 amount of construction waste was dumped in the pit and four slope benches were built at the exit of the pit
153 (Fig. 8e). The volume of the waste increased significantly with the first and second benches completed in
154 late 2014, and the third to fifth benches were still under construction until Jan 2015 (Fig. 8f).
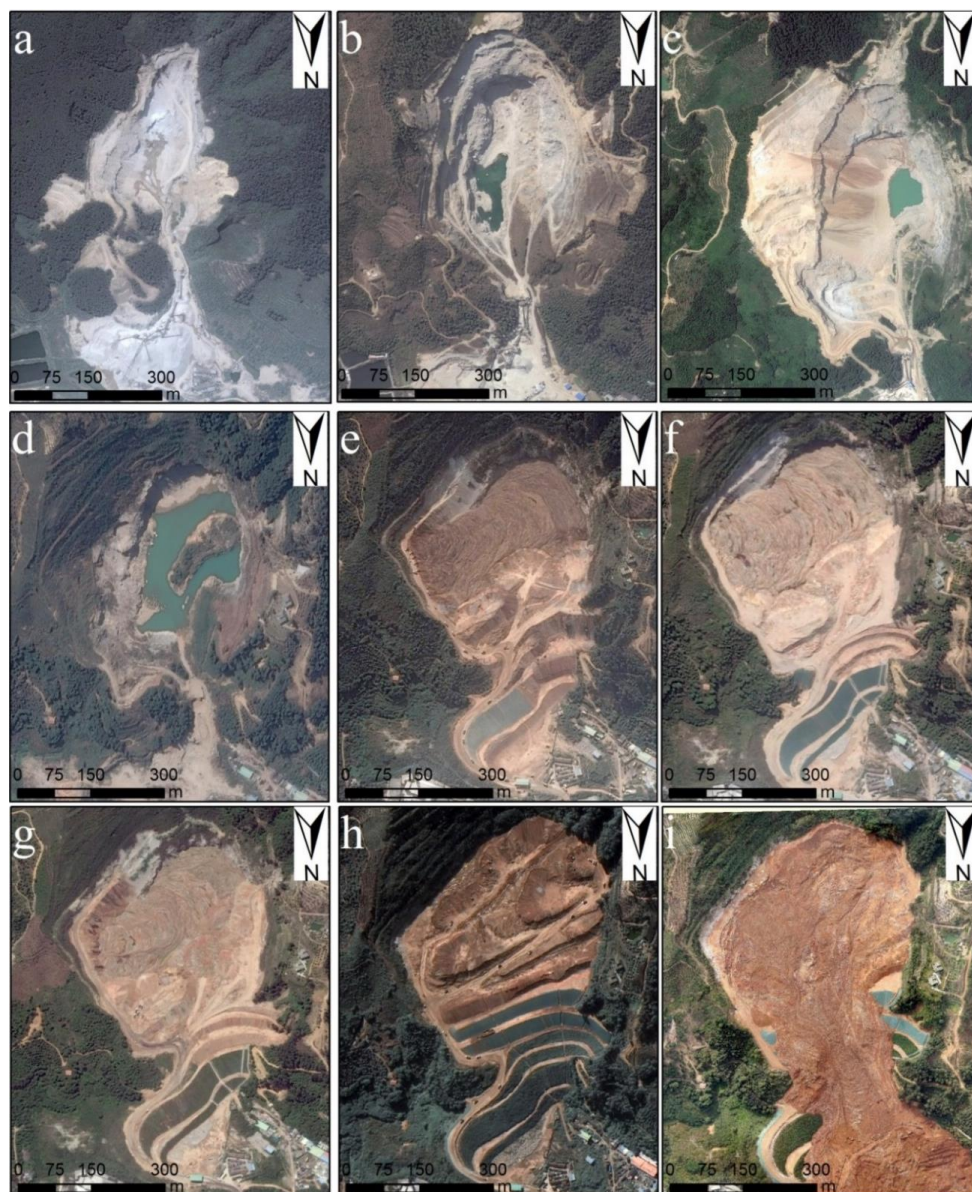
155

156 Fig. 8 Multi-temporal remote sensing images of the study area. **a** 08/31/2002; **b** 02/20/2008; **c** 08/30/2010;
157 **d** 11/25/2013; **e** 11/17/2014; **f** 01/23/2015; **g** 04/14/2015; **h** Pleiades (12/18/2015); **f** Aerial (12/23/2015).
158 Image **a** to **g** were obtained from Google Earth. A service road was excavated at the exit of the quarry with
159 a width of nearly 70 m (see image **a**, **b**, **c**, and **d**).

160 The rapid accumulation and total volume of the waste filling in the dumpsite gained some concerns before
161 the flowslide. An environmental assessment provided by a third-party consulting firm warned the erosion
162 at the site and its influence on the slope stability in Jan 2015 (Zou 2016). The disposal activity was ceased
163 for a certain period as no trucks were seen in the daylight (Fig. 8f). The cease was verified by the interview
164 with the local inhabitants. The disposal activity was resumed in or before April 2015, and the fourth bench
165 was completed as shown in Fig. 8g. By comparing Fig. 8g and Fig. 8h, significant modifications on the
166 landform can be seen in the study area with major increase in volume of the waste filling as the height of
167 the landfill was close to the crest of the quarry pit. The waste filling was flattened and disposal activity was
168 intense as more than 20 trucks appeared in Fig. 8h. Seven additional benches were completed with surface
169 drainage channels installed on the hillslope, and the eighth bench was still under construction during the
170 flowslide. The thickness of the dumpsite was estimated as 90 m with total volume of $6.3 \times 10^6 \, \mathrm{m}^3$ (Fig. 9a)
171 by extracting the difference between the pre- and post-filling DEMs.
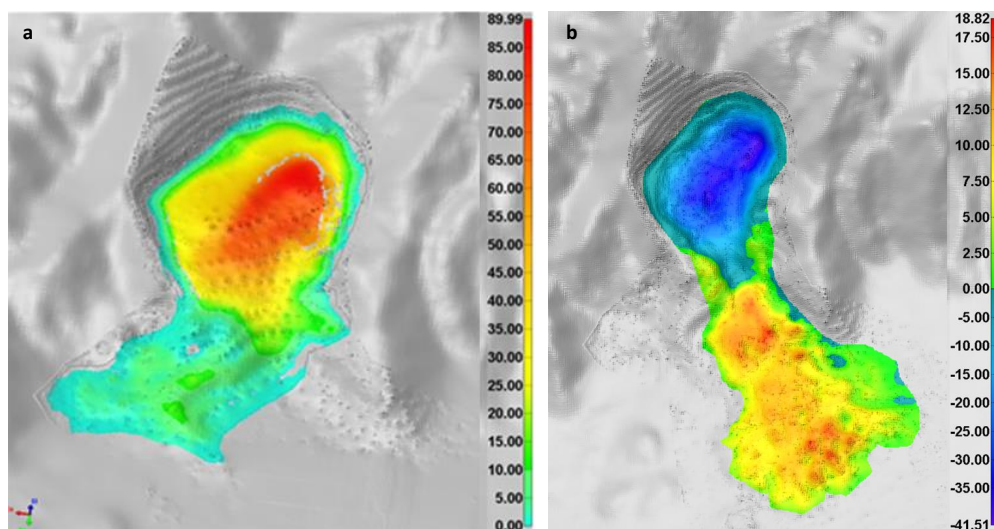
173 Fig. 9 **a** The thickness distribution of the dumpsite based on the pre-/post-disposal DEMs; **b** The elevation
174 variations of the dumpsite estimated between the pre-/post-sliding DEMs.

175 **5 Flowslide Characteristics**

176 The flowslide area can be divided into the source area and flow-accumulation area as shown in Fig. 10. The
177 source area was the pit of the abandoned quarry pit. The mass slid in the direction of nearly 340° with the
178 maximum traveling distance of 1203 m. The maximum thickness of the remaining material in the source
179 area was 41.51 m with an average of 20.5 m (Fig.11 and Fig. 12). The maximum deposit thickness in the
180 flow-accumulation area was 18.2 m with an average of 8.21 m (Fig. 9b). The geometric characteristic of
181 the flowslide can be expressed in length (L), height (H), width (W), and area (S) (Scheidegger 1973; Legros
182 2002). The geometric parameters are indicated in the simplified flowslide geometry in Fig. 13 with values
183 listed in Table 1, Table 2 and Table 3.

184
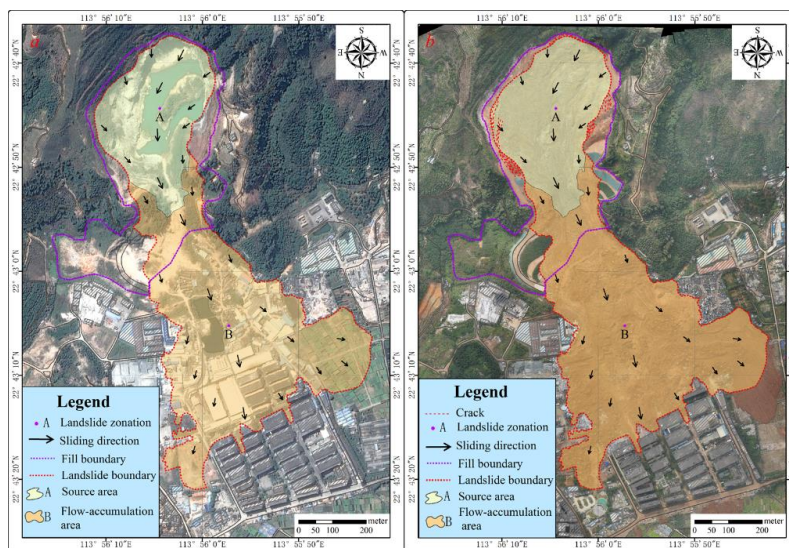
185 Fig.10 The direction of flowslide and distribution of the displaced material. **a** Flowslide overlying the pre-
186 sliding industrial park showing the impact area and flow direction; **b** Aerial view of the flowslide.
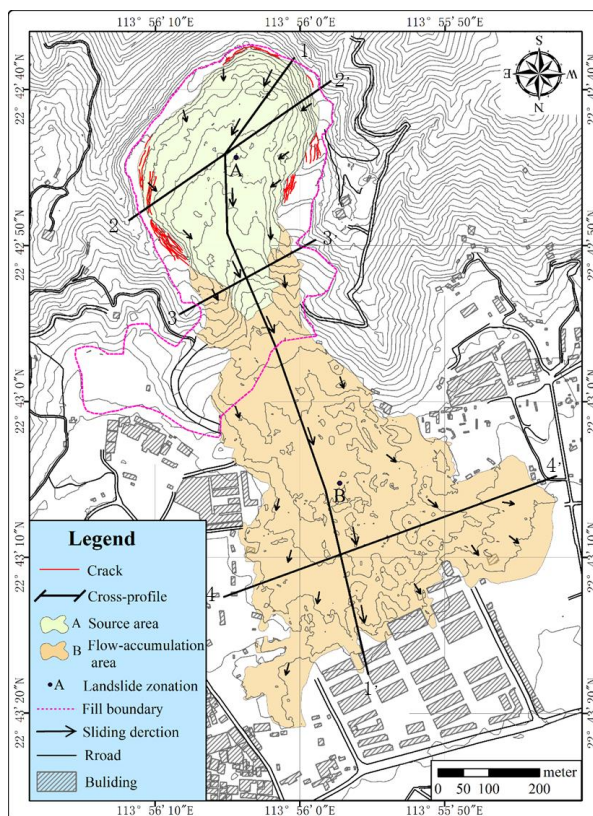
187

188 Fig.11 The topographic map of the flowslide.
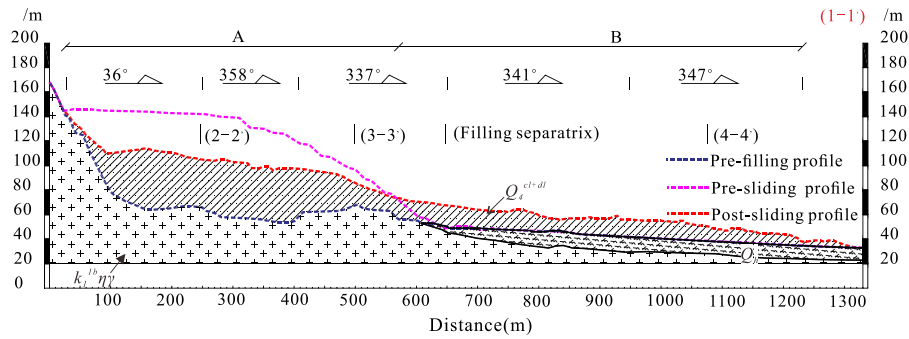
189

190   Fig.12 The geological and topographical cross section (profile line 1-1')
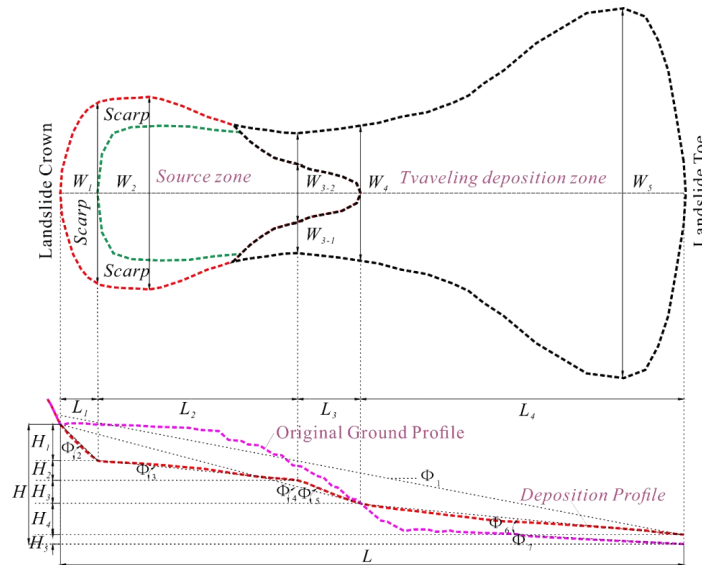
191

192   Fig. 13 Simplified illustration of the flowslide geometry. L: run-out distance; H: elevation; W₁: scarp width;
193   W₂: max width of the source area; W₃: frontal width of the source area; W₄: width of the shear crack; W₅:
194   max width of the flow-accumulation area; L₁: horizontal length of the scarp; L₂: horizontal length of the
195   mild slope; L₃: horizontal length of the steep slope; L₄: horizontal length of the flow-accumulation area; H₁:
196   height of the scarp; H₂: height of the mild slope; H₃: height of the steep slope; H₄: height of the flow-
197   accumulation area; H₅: thickness of the toe of the flowslide; Φ₁: extension angle; Φ₂: slope gradient of the
198   scarp; Φ₃: mild slope gradient; Φ₄: slope gradient of the source area; Φ₅: steep slope gradient; Φ₆: slope
199   gradient of the flow-accumulation area; Φ₇: slope gradient of the foundation area

200   Table 1 Geometric parameters of the flowslide (Length and Width)

Parameter	L (m)	H (m)	W₁ (m)	W₂ (m)	W₃₋₁ (m)	W₃₋₂ (m)	W₄₋₁ (m)	W₄₋₂ (m)	W₅ (m)
Value	1204.67	111.31	212.5	399.32	218.31	149.38	217.71	64.63	592.25

201   Table 2 Geometric parameters of the flowslide (Angle)

Parameter	Φ₁ (°)	Φ₂ (°)	Φ₃ (°)	Φ₄ (°)	Φ₅ (°)	Φ₆ (°)	Φ₇ (°)	K	S (m²)
Value	5.28	28.06	1.2	7.62	11.36	3.08	1.36	0.32	398619.6

202 Table 3 Geometric parameters of the flowslide (Area and Thickness)

Parameter	Area A	Area B
S (m^2)	11.35×10^4	28.51×10^4
V (m^3)	2.32×10^6	2.34×10^6
T_{max} (m)	41.51	18.82
T_{ave} (m)	20.49	8.21

203 **5.1 Source Area**

204 The source area of the flowslide is the quarry pit with a length (L_{1+2+3}) of 540.30 m and a width (W_2) of
205 399.32 m. The area of the source area (S_A) is 11.35×10^4 m^2 and the height (H_{1+2+3}) was 68.5 m with an
206 apparent dip (Φ_4) of 7.62° (Fig. 14 and Table 1). The volume of the mobilized material in the source area
207 was 2.32×10^6 m^3 and the remained volume was 3.95×10^6 m^3. The maximum thickness of the source area
208 (T_{A-max}) was 41.5 m with an average thickness (T_{A-ave}) of 20.5 m. The scarp located on the west of the main
209 scarp has steep slope gradient with mild gradient on the east. The height of the steep scarp ranged from 25
210 to 47 m, whereas the height of the mild scarp ranged from 10 to 20 m. The geological cross section (profile
211 line 2-2') of the source area is shown in Fig. 14. The maximum thickness of the source area was 40.65 m
212 with an average of 34.83 m. The overview of the source area is shown in Fig. 15, with details on the
213 remaining material presented in Fig. 16.

214
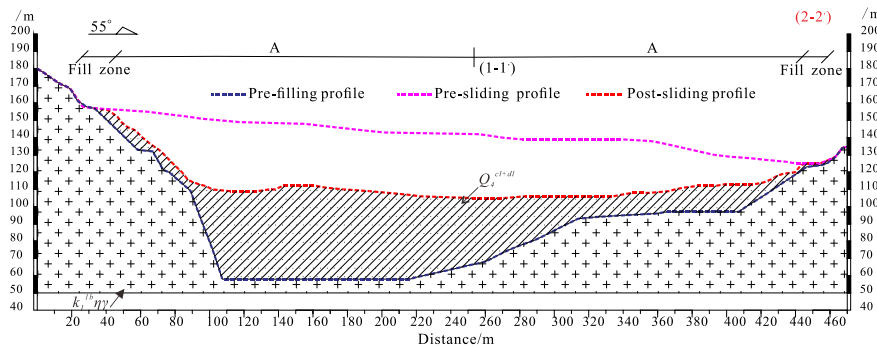
215 Fig.14 The geological cross section (profile line 2-2') of the source area.

216 With the ingress of rainwater and groundwater in the dumpsite, pore water pressure increases due to the
217 low permeability of the underlying granite in the Cretaceous system. It is appeared that the lack of drainage
218 resulted in waste filling saturation in the lower portion of the dumpsite, which in turn formed the sliding
219 bed of the flowslide (Fig. 15 and Fig. 16).
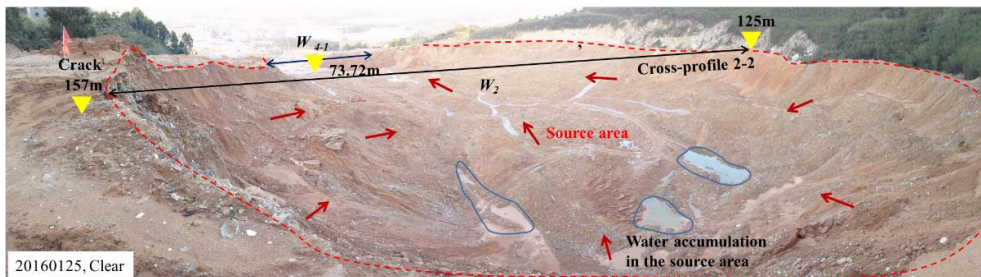
220

221 Fig.15 An overview of the source area (image taken at the flowslide crown facing north). A large opening
222 (W_{4-1}) formed due to the failure of the retaining slope (the exit of the original quarry pit), which provided
223 passage for the flowslide and permitted rapid release of kinematic energy.

224 A large amount of silty soil were observed in the source area (Fig. 16). It is postulated that the material on
225 both sides of the source area were mobilized due to the debuttressing effect as the waste filling in the lower
226 portion of the dumpsite slid into the downstream industrial park, and in consequence, resulted in the collapse
227 of the dumpsite. Step-like steep scarp was formed on the west part of the main scarp area (Fig. 17c and
228 17d), with tensile cracks developed on the rear edge as well as both sides of the scarp.
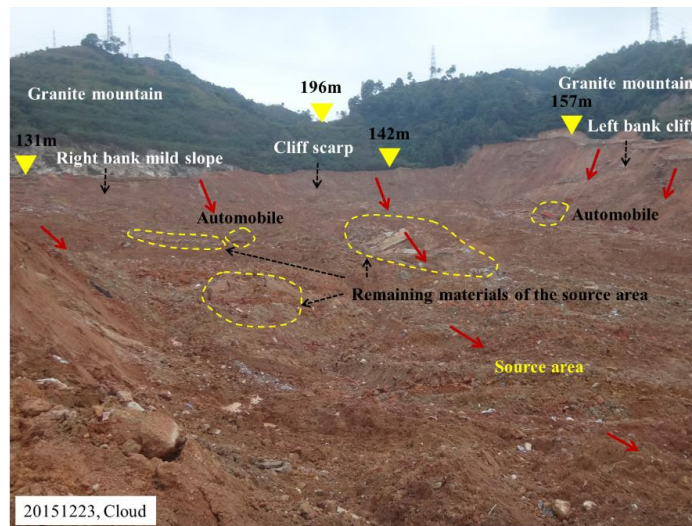
229
230 Fig.16 An overview of the remaining material in the source area (image taken near the quarry pit exit facing
231 south). Several service vehicles parked in the rear edge of the dumpsite were dragged into the source area
232 as waste filling slide into the industrial park. Blocky rock fragments were found in the source area.
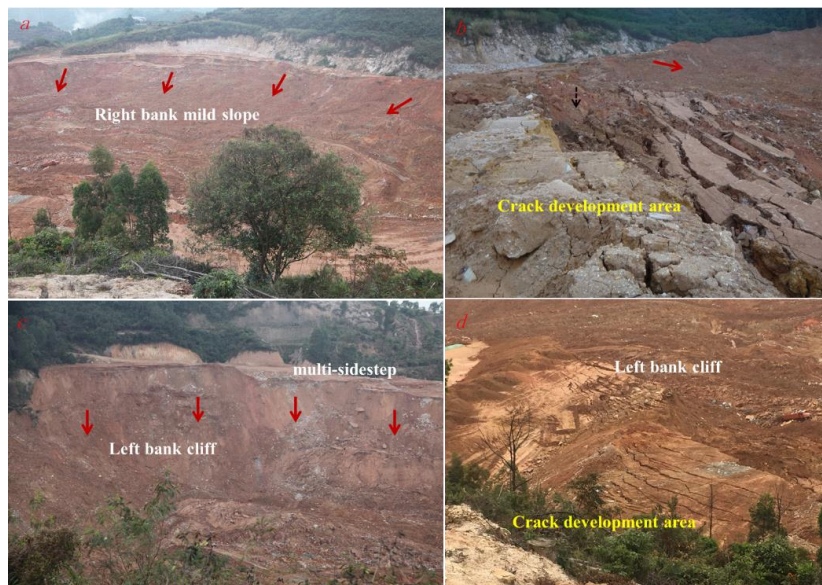
233
234 Fig.17 Characteristics of the remaining material in the source area. **a** Mild scarp on the east part of the main
235 scarp area; **b** Cracks were developed in the west boundary of the flowslide; **c** Step-like steep scarp on the
236 west part of the main scarp area; **d** An overview of the west part of the flowslide crown.

237 The presence of the aforementioned rock hills formed unfavorable topography for retaining slope stability
238 by promoting a narrow gully for groundwater flow (Fig. 8c and Fig. 10b). As a result of the retaining slope
239 failure, a large opening was formed at the elevaton of 73.7 m between the front edge of the steep scarp and
240 the rear edge of the flow-accumulation area as shown in Fig. 11, Fig. 12, and Fig. 15. The displaced material
241 was stratified in the middle part of the flow-accumulation area during the high speed sliding process. The
242 shape of the failed retaining slope was half-elliptic-like with a width (W_{4-1}) of 217.7 m and a height (H_b) of
243 27.5 m (Fig. 18 and Fig. 19).
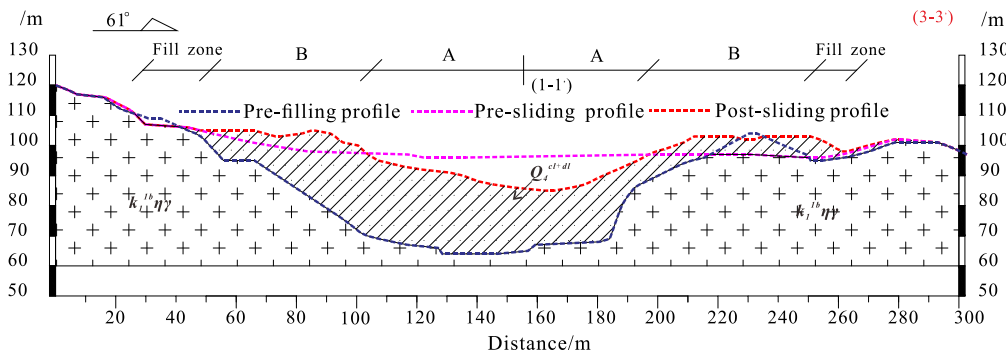
244
245 Fig. 18 Geological cross section (profile line 3-3') of the failed retaining slope located at the original quarry
246 pit between the two rock hills.
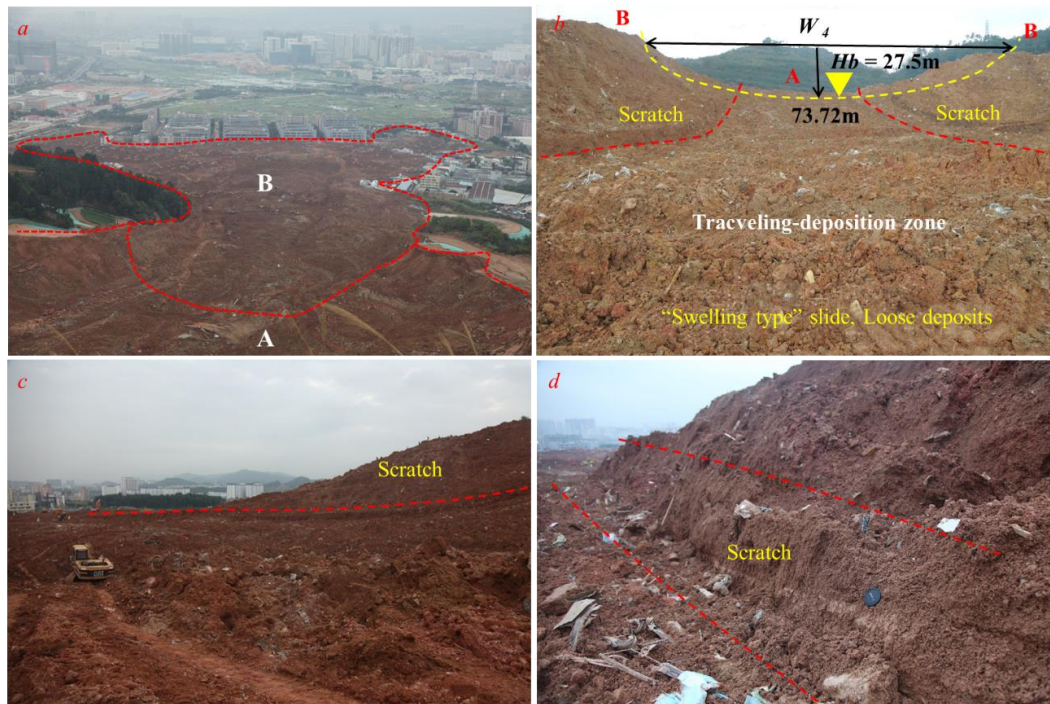
247
248 Fig. 19 **a** An overview of the exit of the flowslide between the source and flow-accumulation area (Photo
249 courtesy of China News Agency); **b** The half-elliptic-like opening of the failed retaining slope; **c** East side
250 of flow-accumulation area adjacent to the opening showing scratch caused by the flowslide; **d** Details on
251 the scratches.

252 **5.2 Flow-Accumulation Area**

253 The fan-shaped flow-accumulation area mantled the retaining slope of the dumpsite and a large part of the
254 industrial park as shown in Fig. 20. The original slope gradient of the industrial park (Φ) was 1.36° along
255 the profile line 1-1' as shown in Fig. 14 and Table 1. The area immediately downstream of the landfill was
256 relatively flat with no major construction except a pond (approx. 3600 m^2) and a channel (width: 7 m and
257 length: 130 m). Most of the industrial structures were constructed on east, west, and north side of the pond
258 as shown in Fig. 10a, and therefore, created a ideal flow channel for the mass movement. The failure of the
259 rock retaining slope resulted in an opening for the waste fill flow and destoryed downstream bluildings (Fig.
260 20 and Fig. 21).
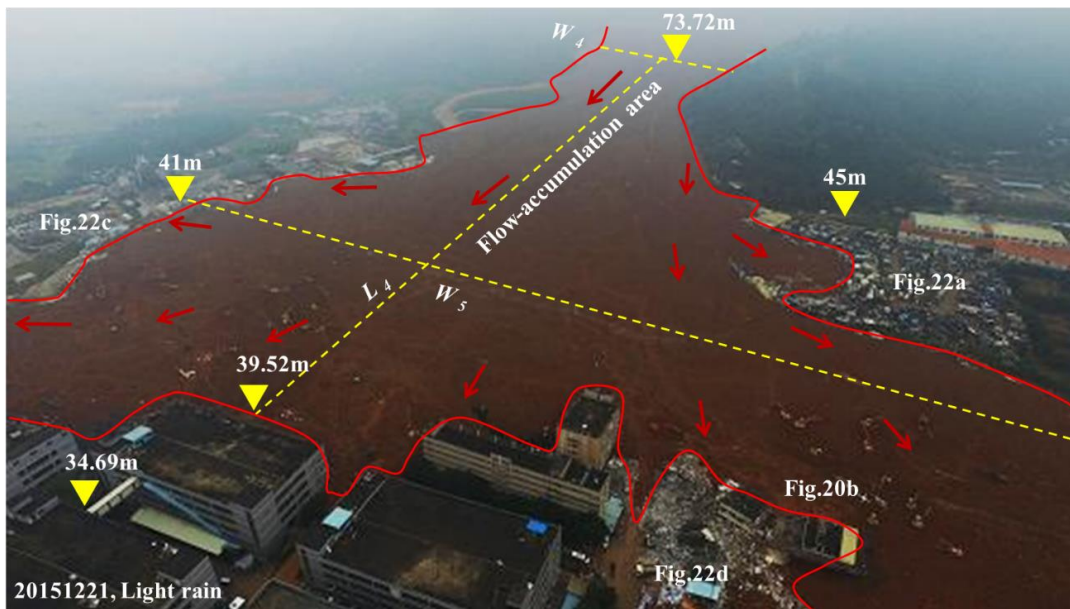
261

262 Fig. 20 The overview of the flow-accumulation area with elevations (Photo courtesy of China News Agency)
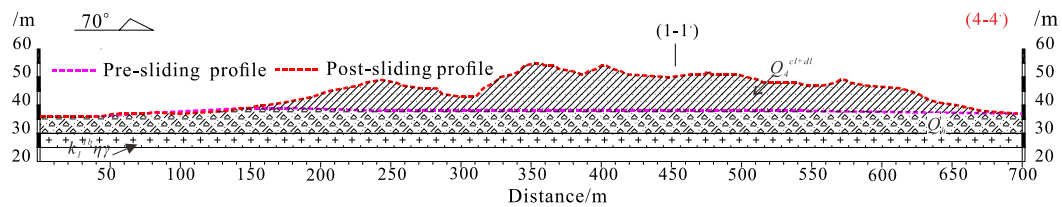
263

264 Fig. 21 Geological cross section (profile line 4-4') of the flow-accumulation area. The length (L_4) was 664.4
265 m and the width (W_3) was 218.3 m with the width of the front edge (W_5) of 592.3 m. The area of the flow-
266 accumulation area is 28.51×10^4 m^2 and the elevation difference (H_4) was 35.7 m with the apparent dip (Φ_6)
267 of 3.08°. The average thickness in the flow-accumulation area was 8.21 m with the maximum thickness of
268 18.82 m (Fig. 14, Table 1, and Table 3).
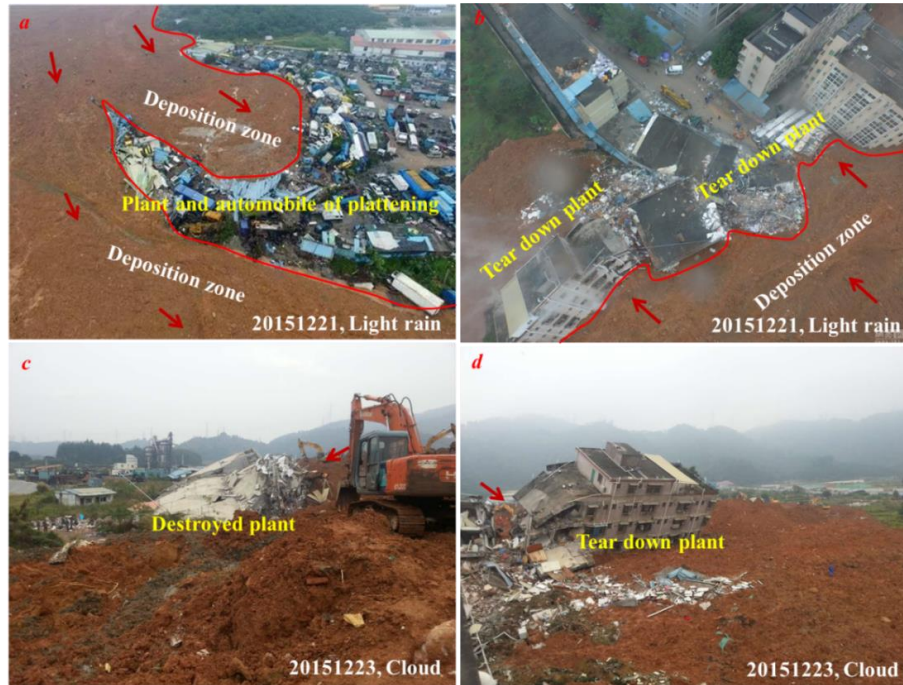
269

270   Fig. 22 The damage of buildings in the industrial park (Photo courtesy of China News Agency).

271   **5.3 Flowslide Movement**

272   The source area of the flowslide was in the elevation of 142 m and the horizontal run-out distance (L) was
273   approximately 1203 m, with the elevation difference (H) of 111 m. The sliding velocity can be estimated
274   on the basis of the landslide geometrical characteristics. The velocity of the high-speed landslide can be
275   estimated using the following expression (Scheidegger 1973):

$$v = \sqrt{2g \times (H - f \times L)} \tag{1}$$

276   Where v is the sliding velocity (m/s), g is the gravitational acceleration (m/s^2), H and L is the elevation
277   difference and horizontal distance (m) between the crown and toe of the flowslide, respectively, and f is the
278   equivalent friction coefficient referred as the ratio between the height and run-out distance of the flowslide
279   (f = H/L). The equivalent friction coefficient of the dumpsite flowslide is 0.092. The relations of the run-
280   out distance, elevation difference, and equivalent friction coefficient can be defined in light of the flowslide
281   geomoetry (Fig. 13). The sliding velocity was calculated and presented in Fig. 23.
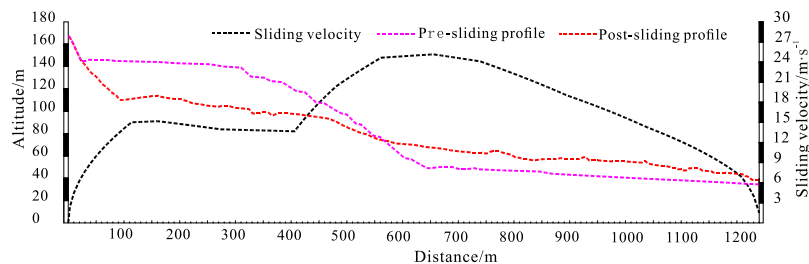
282

283   Fig. 23 The relationship between sliding velocity along profile line 1-1' and pre-/post-sliding landform.

284   Based on the calcuated sliding velocity profile, two sharp increases in the velocity can be seen, including
285   the movement of the waste filling near the steep scarp and the acceleration of the flowslide exiting the pit.
286   The sliding velocity of the mass accelerated to 15.17 m/s as waste filling reached the bottom of the steep
287   scarp. The velocity displaced material gradually decreased to approximately 13 m/s before accelerate to the
288   maximum velocity of 25.15 m/s as it reached to the opening of the dumpsite. The second sharp acceleration
289   was followed by ripid dissipation of kneimatic energy and reduction on the velocity as it reached the flow-
290   accumulation area (elev. 50 m). It was estimated that the sliding velocity was reduced to 15.68 m/s when it
291   made contact with downstream buildings, and then ceased moving due to the obstruction of structures. The
292   geometry and velocity exhibited the characteritics of high-speed long run-out flowslide.

293   **6 Laboratory Experiment**

294   Based on *in-situ* tests for waste filling density and moisture content as well as the laboratory compaction
295   test, it was found that the dry density varies from 1.25 to 1.48 g/cm^3 and void ratio ranged between 0.83
296   and 1.31. Standard compaction test results suggested that the optimal water content of the waste filling was
297   15.31% with the highest dry density of 1.79 g/cm^3. The surface of the waste filling was in loose state with
298   degree of compaction of the dumpsite ranged from 69.83% to 82.68%. Undrained shear test estimated that
299   c and Φ of the waste filling is 4.7 kPa and 31.9°, respectively (Fig. 24), which is considerbly higher than
300   gradient of the retaining slope.
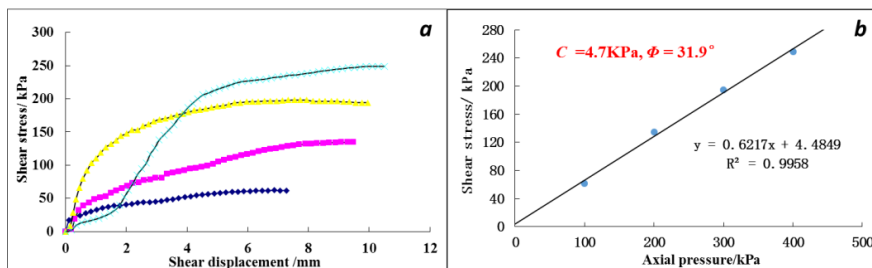
301

302   Fig. 24 Shear strength of the waste filling specimen obtained by undrained shear test.

303   **7 Numerical Analysis**

304   The numerical analysis aims at inverse analyzing the friction angle of the waste filling under the occurrence
305   of the flowslide. Dumpsite slope FoS was estimated by using SLOPE/W software with Morgenstern Prince
306   Limit Equilibrium Analysis method. Since tt is postulated that the sliding mass in the lower portion of the
307   dumpsite was saturated prior to the flowslide, a hypothetic sliding surface and the groundwater level were
308   added into the model. The FoS was determined with an iterative approching by changing the postion of the
309   sliding surface until failure of the dumpsite (Fig. 25 and Fig. 26). The physical parameters for the model
310   were determined by the laboratory experiments and inversion analysis (Table 4).

311
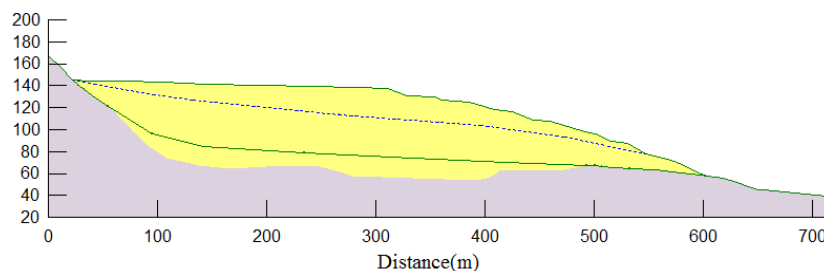
312   Fig. 25 Hypothetic sliding surface (green solid line) and groundwater level (blue dash line) in 2D numerical
313   model.
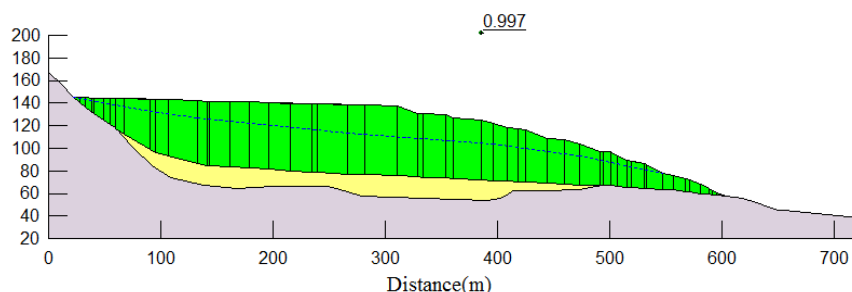
Fig. 26 Estimated FoS for the 2D numerical model.

Table 4 Material properties and parameters for the model

	Laboratory Experiment			Inversion Analysis		
	Unit Weight (kN/m^3)	c (kPa)	Φ (°)	Unit Weight (kN/m^3)	c (kPa)	Φ (°)
Waste Filling	16.5	-	-	16.5	-	-
Waste Surface	-	5	31	-	5	9.4

The results of slope stability analysis is presented in Table 5. Based on the numerical analysis, it was found possible for the development of a sliding surface above the bedrock in the lower portion of the waste filling. It is evident that the permeability of the waste filling was considerably low, which may result in saturation in the lower portion of the waste filling. As no clear drainage passage were found for the waste filling, the displaced material may remain undarined during the flowslide so that the shear strength was significantly reduced. The substaintial difference in the shear parameters obtained from laboratory test and numerical analysis indicated that the conventional numerical analysis is not appropriate for analyzing the failure mechanism of the flowslide. Additionally, the uncertainty of groundwater condition affects the analysis.

Table 5 Results of the numerical slope stability

Parameters	Unit Weight (kN/m^3)	c (kPa)	Φ (°)	FoS
Value	16.5	5	9.4	0.997

8 Discussion and Conclusion

The topography of the flowslide has the following features: (1) Suitable topography with a height of 124 m between the crown and toe of the flowslide which stored large potential energy needed for high speed and long run-out distance flowslide; (2) Low permeability of the waste filling in the dumpsite with impermeable bedrock resulted in groundwater stagnation. However, the failure of the retaining slope formed a narrow opening for the subsequent flowslide, with sudden release of high kinematic energy generating high sliding velocity and long travel distance.

Since the parameters obtained by the inversion analysis were largely different from the experimental results, it is postulated that the deformation and failure of the landfill was ascribed to the excess pore water pressure in the waste filling. The sharp increase of the pore water pressure causes significant destruction and results in liquefaction. Localized liquefactions were found at several locations on the study area (Fig. 27). The exact reason for the surge in the pore water pressure remains unclear at this point, however, it may involve: (1) rapid surcharge loading in the dumpsite while pore water pressure cannot dissipate immediately; (2) the waste filling was loosely packed with large pores in the microstructure, and the collapse of particle structure lead to the shrinkage of pores, and in turn building excess pore water pressure.

341

342   Fig. 27 Evidence of liquefaction near the opening of the failed retaining slope.

343 The engineering background of the dumpsite prior to the event include mainly three phases, i.e. the mining
344 process of the quarry, construction of the downstream industrial zone, and waste filling process. However,
345 the previous engineering undertakes posed very limited influnence on the stability of site, and based on the
346 field investigations, the volume of the waste filling was estimated as 6.27×10^6 m^3, which was three times
347 larger than the design capacity of the dumpsite.

348 The dumpsite flowslide is divided into the source area and flow-accumuation area. The volume of the source
349 area was 2.32×10^4 m^3 with the max. and average thickness of 41.5 m and 20.5 m, respectively. The volume
350 of the fan-shaped flow-accumulating area was 2.34×10^6 m^3 with the max. and average thickness of 18.8 m
351 and 8.2 m, respectively. The volume expansion coefficient of flowslide was 1.007. The maximan sliding
352 velocity of the flowslide was 25.15 m/s at the opening of the dumpsit, and reduced to 15.68 m/s as it reached
353 the industrial park and ceased moving due to the obstruction of buildings. The flowslide is charcteristiced
354 by high speed and long run-out distance. The laboratory test and numerical model yielded largely different
355 results for the shear strength of the waste filling. Meanwhile, field investigation indicated liquidation at
356 several locations on the site. Unregularly disposal activites in addition to the ingress of rainwater and high
357 pore water pressure played important roles in deformation process of the dumpsite. Although the flowslide
358 destruction process was fast with excessive amount of waste filling accumulation, it is postulated that signs
359 of deformation may have already appeared in the study site but not discovered due to the absence of field
360 monitoring. Further analysis is undergoing at SKLGP to assess the causes involoved for generating the
361 excess pore water pressure.

362 **Acknowledgments** The work is financially supported by the NSFC (Grant No. 41521002) and the National
363 State Key 973 Project (Grant No. 2014CB744703) from the Ministry of Science and Technology of the
364 People's Republic of China.

365 **Reference**

366 Blight G (2008) Slope failures in municipal solid waste dumps and landfills: a review. Waste Manag Res
367   26:448–463. doi: 10.1177/0734242X07087975

368   Blight GE, Fourie AB (2005) Catastrophe revisited–disastrous flow failures of mine and municipal solid
369   waste. Geotech Geol Eng 23:219–248.
370   Brunner PH, Fellner J (2007) Setting priorities for waste management strategies in developing countries.
371   Waste Manag Res 25:234–240. doi: 10.1177/0734242X07078296
372   Chang M (2002) A 3D slope stability analysis method assuming parallel lines of intersection and differential
373   straining of block contacts. Can Geotech J 39:799–811. doi: 10.1139/t02-020
374   Chang M (2005) Three-dimensional stability analysis of the Kettleman Hills landfill slope failure based on
375   observed sliding-block mechanism. Comput Geotech 32:587–599.
376   Chen Z, Yuan J (2009) An Extended Environmental Multimedia Modeling System (EEMMS) for Landfill
377   Case Studies. Environ Forensics 10:336–346. doi: 10.1080/15275920903347396
378   Chugh AK, Stark TD, DeJong K a (2007) Reanalysis of a municipal landfill slope failure near Cincinnati,
379   Ohio, USA. Can Geotech J 44:33–53. doi: 10.1139/t06-089
380   Dai Z, Huang Y, Jiang F, Huang M (2016) Modeling the flow behavior of a simulated municipal solid
381   waste. Bull Eng Geol Environ 75:275–291. doi: 10.1007/s10064-015-0735-8
382   Daouadji A, Hicher P (2010) An enhanced constitutive model for crushable granular materials. Int J Numer
383   Anal Methods Geomech 34:555–580.
384   Eid HT, Stark TD, Evans WD, Sherry PE (2000) Municipal solid waste slope failure. I: Waste and
385   foundation soil properties. J Geotech Geoenvironmental Eng 126:397–407.
386   Huang Y, Cheng H (2016) A simplified analytical model for run-out prediction of flow slides in municipal
387   solid waste landfills. Landslides (Published:1–9. doi: 10.1007/s10346-016-0688-4
388   Huang Y, Dai Z, Zhang W, Huang M (2013) SPH-based numerical simulations of flow slides in municipal
389   solid waste landfills. Waste Manag Res 31:256–64. doi: 10.1177/0734242X12470205
390   Huvaj-Sarihan N, Stark TD (2008) Back-Analyses of Landfill Slope Failures. 6th Int Conf Case Hist
391   Geotech Eng 1–7.
392   Kjeldsen P, Fischer E V (1995) Landfill gas migration - field investigations at Skellingsted landfill,
393   Denmark. Waste Manag Res 13:467–484.
394   Kocasoy G, Curi K (1995) The Ümraniye-Hekimbaşi open dump accident. Waste Manag Res 13:305–314.
395   Lavigne F, Wassmer P, Gomez C, et al (2014) The 21 February 2005, catastrophic waste avalanche at
396   Leuwigajah dumpsite, Bandung, Indonesia. Geoenvironmental Disasters 1:1–12. doi:
397   10.1186/s40677-014-0010-5
398   Legros F (2002) The mobility of long-runout landslides. Eng Geol 63:301–331.
399   Merry SM, Kavazanjian Jr E, Fritz WU (2005) Reconnaissance of the July 10, 2000, Payatas landfill failure.
400   J Perform Constr Facil 19:100–107.
401   Mitchell JK, Seed RB, Seed HB (1990) Kettleman Hills waste landfill slope failure. I: Liner-system
402   properties. J Geotech Eng 116:647–668. doi: 10.1061/(ASCE)0733-9410(1990)116:4(647)
403   Nicot F, Darve F (2011) Diffuse and localized failure modes: two competing mechanisms. Int J Numer
404   Anal Methods Geomech 35:586–601.
405   Scheidegger AE (1973) On the prediction of the reach and velocity of catastrophic landslides. Rock Mech
406   Rock Eng 5:231–236. doi: 10.1007/BF01301796
407   Srour G (2011) Mine waste failure: an analysis of empirical and graphical runout prediction methods.
408   University of British Columbia
409   Yılmaz A, Atmaca E (2006) Environmental geological assessment of a solid waste disposal site: a case
410   study in Sivas, Turkey. Environ Geol 50:677–689.
411   Zhang Y, Qi M, Ma H (2006) Slope instability and its control in Shenzhen City. Chinese J Rock Mech Eng
412   S2 (in Chinese).
413   Zhao C, Dai F (2007) Study on failure mechanism of a fill slope in Shenzhen. Chinese J Geol Hazard
414   Control 18:3412–3421 (in Chinese).
415   Zou DH (2016) Exploring a Waste Dump Site Failure–Possible Causes and Prevention Measures. Int J
416   Geohazards Environ 2:25–33.
417